Spectator-electron behavior during cascade decay in krypton

G. B. Armen,[1] E. P. Kanter,[2] B. Krässig,[2] J. C. Levin,[1] S. H. Southworth,[2] and L. Young[2]
[1]*Department of Physics, University of Tennessee, Knoxville, Tennessee 37996, USA*
[2]*Argonne National Laboratory, Argonne, Illinois 60439, USA*
(Received 18 December 2003; published 14 June 2004)

We report new measurements of Kr^{q+} photo-ions, coincident with $K\alpha$ or $K\beta$ fluorescence as incident-photon energy is swept through the Kr *K*-shell threshold. From the branching ratios just above threshold, we obtain measurements of the ion charge-state probabilities for decay from the Kr $[2p]$ and Kr $[3p]$ states. In the threshold region, we observe both resonant enhancement and depletion of the branching ratios. By analyzing this behavior in light of theory, we extract sticking probabilities, which we feel are a useful set of parameters for investigating the general relationship between cascade decay from resonant and nonresonant hole states. A simplified theoretical model is employed to calculate these probabilities for the Kr^{2+} and Kr^{3+} cases.

DOI: 10.1103/PhysRevA.69.062710 PACS number(s): 32.80.Hd, 32.50.+d, 32.80.Fb

I. INTRODUCTION

When a photon of sufficient energy encounters an atom it can be scattered inelastically, leaving the atom in an excited state. The process of radiative resonant Raman scattering [1–3] is an example of such inelastic x-ray scattering. In particular, when the incident photon energy is near the atomic *K*-shell threshold, the atom can be left in an ionized state with a hole an electronic shell *i*—which we denote as $[i]$. In this case, due to the resonant nature of the problem, the ejected electron and scattered photon leave with characteristic energies. This process (sometimes referred to as continuous Raman scattering) evolves into the familiar fluorescence process for energies larger than threshold. Near threshold, the atom may also be left in an excited, neutral state containing a hole in the shell *i* and an excited electron bound in a Rydberg orbital *nl*—denoted by $[i]nl$. In this process (sometimes referred to as resonant fluorescence) the scattered photon also has a characteristic energy near to that of the ionized case.

For lower energies, these characteristic x rays (fluorescence lines) can give direct information about the dynamics of the Raman process near threshold (see, e.g., [4]). For processes involving larger energy however, such as the *K*-shell of the heavier atoms, this becomes unfeasible: the width of the lines become very much larger than their separations. A possible solution to this problem is to monitor the ions produced. If the hole lies below the valence level, then the ensuing cascade decay will produce an ion charge-state spectrum which depends on the initial cascade state, i.e., $[i]$ or $[i]nl$. Presumably, decay from the neutral states will result in lower charge states, so that a study of ion yields should give some information about the production process. To be more precise, one must therefore know how such charge-state spectra are affected by the presence of an externally bound Rydberg electron.

In a previous work [5] (referred to hereafter as "Part I") we have made a preliminary investigation of this idea: the yield of Kr^{q+} ions was recorded in coincidence with unresolved $K\alpha$, $K\beta$ fluorescence for incident-photon energies across the *K*-shell edge. Experimentally, we found that indeed the yields of low-*q* ions were enhanced at the expense of high-*q* ions near threshold. Furthermore, this relative enhancement provided a (rough) view of the resonant-fluorescent cross section, when suitably interpreted. In seeking to understand this behavior, we developed a simplified model of cascade decay from the resonant states $[i]nl$, based on the nature of decay from the ionized state $[i]$. The outgrowth of this model was the concept of "sticking probabilities," whose validity is actually more general than the proposed model. In Part I we were able to extract these parameters from the experiment and, descriptively using our model, make a case for the trends observed.

The present work is an extension of our previous work in several ways: Using a new method, we have repeated the experiment with a smaller bandpass, while now distinguishing between $K\alpha$ and $K\beta$ coincidences. The new data thus fall into two sets, corresponding to decay from $2p$ and $3p$ hole states. From this we extract sticking probabilities—which no longer reflect an average over initial states. The method of analysis is improved over the previous one. Finally, we also apply our theory to a few tractable cases, attempting to establish the validity of the proposed model.

The present work relies to some degree on that of Part I, and we seek here to create a reasonably self-contained report, while avoiding as much repetition of the previous paper as possible. In Sec. II we discuss the experimental method, dwelling on the new aspects. In Sec. III we present an outline of the theory sufficient for present needs. In Sec. IV the data is presented and analyzed, using a new method which minimizes the dependence on unknown (and hence theory-dependent) quantities. Section V examines these results in light of the theory.

II. EXPERIMENTAL METHODS

The experiment was performed on the BESSRC-CAT wiggler beamline 11-ID-D [6] at the Advanced Photon Source, Argonne National Laboratory. The synchrotron radiation was monochromatized using a Si (220) double crystal monochromator. Using a 0.5 mm slit between the monochromator and the focusing mirror, the bandpass was estimated as

2.5 eV at the Kr *K*-edge (14.326 keV)—half that of our previous experiment.

As before, the incident x rays were focused onto a Kr gas jet, located at the source region of both an ion time-of-flight (TOF) spectrometer and an x-ray fluorescence detector. Background pressure in the chamber was maintained at 6×10^{-5} torr (corrected ion-gauge reading) by applying a 5 torr backing pressure to the gas needle with a Baratron metering system.

Ions created in the source region were accelerated electrostatically in the TOF spectrometer to energies of 2.5 keV/q and detected by Z-stacked microchannel plates (MCP) biased at 3 kV. X rays emitted in the source region were detected with a Si(Li) detector. The Si(Li) detector was mounted at right angles to the plane of polarization, located approximately 1 cm from the source region with an entrance diameter of 1 cm, providing a solid angle of ~6% of the total sphere.

Data were recorded in event mode. The use of the Si(Li) x-ray detector in the present experiment allowed for the discrimination of both $K\alpha$ and $K\beta$ fluorescence. These x-ray events were also used to establish the start time for the ion TOF detector. The slow rise time of the Si(Li) pulses would have resulted in a statistical spread of ~40 ns in the start time, which was comparable to the Kr^{q+} peak separations. Hence, the resolution of the coincident ion charge-state spectrum would be seriously degraded. To overcome this difficulty, the ring marker signal was also monitored. This signal had a fixed phase relation with the synchrotron x-ray pulses (<80 ps in width), whose separation of 153 ns (singlets) was long in comparison with the Si(Li) pulse spread. Hence each event could be identified (in real time) with a specific pulse, determining a corrected ion start time. Using these corrections, the ion spectra were determined with a resolution inherent to the TOF detector. Setting coincidence windows in the fluorescent x-ray energy then produced high-resolution Kr^{q+} TOF spectra coincident with a specific x-ray fluorescence line. Figure 1 displays typical TOF spectra in which Kr^{q+} ions are measured in coincidence with $K\alpha$ and $K\beta$ fluorescence. Because of the start-time corrections, the peaks are well resolved, showing structure due to the different Kr isotopes. In this work, incident photon energy (denoted E_{edge}) is measured relative to the inflection point of the Kr *K*-edge, as measured in edge scans of the total, non-coincident ion yield. The data of Fig. 1 were recorded at an incident photon energy at this inflection point, i.e., $E_{\mathrm{edge}}=0$.

Because of the low TOF acceleration voltage used in the present experiment, ions of higher charge were detected more efficiently than those of lower charge. To correct for this problem, we employed data from our previous experiment: The earlier data were acquired using a large (5 kV) acceleration voltage and a microsphere-plate detector biased at 3.2 kV, which was believed to have a uniform detection efficiency. To correct the new data, the peak ratios were compared with the old data at four comparable incident energies, above and below threshold. Since the earlier data was coincident with both $K\alpha$ and $K\beta$ fluorescence, care was taken in the comparison to include the differing x-ray detection efficiencies between the $K\alpha$ and $K\beta$ lines for both the present Si(Li) detector and the avalanche photodiode of the previous work. In this way a relative q-dependent detection efficiency could be derived for each of the charge states $q=2,\ldots,8$. Because of the very low yield and detection efficiency for $q=1$, no Kr^{1+} peak was observed in the new experiment.

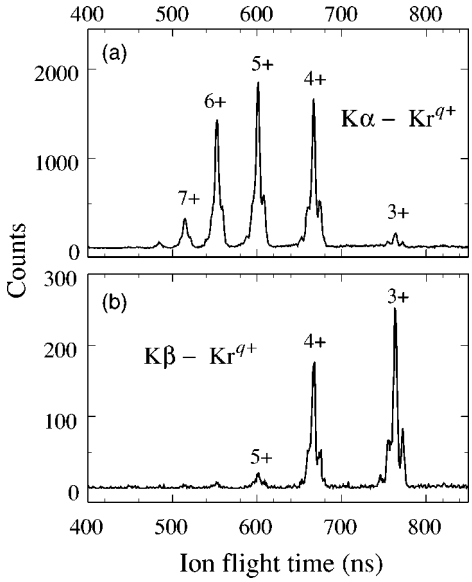

FIG. 1. Kr ion time of flight spectra coincident with $K\alpha$ [panel (a)] and $K\beta$ [panel (b)] x-ray emission. These spectra were recorded with the incident-photon energy set to the inflection point of the observed *K*-shell edge ($E_{\mathrm{edge}}=0$ eV). Each charge peak consists of a number of subpeaks corresponding to the various Kr isotopes.

III. THEORY

This section summarizes the theoretical ideas and definitions needed in the present work. A more complete development is presented in Part I [5].

Consider the cascade decay of an ionized atom (A^+) with a hole in an inner shell i. It decays to a stable ion of charge q with probability P^q:

$$A[i]^+ \xrightarrow{P^q} A^{q+} \quad \text{for} \quad q = q_{\min}, \ldots, q_{\max}, \tag{1}$$

where $q_{\min} \geqslant 1$. We refer to these processes as diagram, or nonresonant, cascade decay paths.

Similarly, cascade decay beginning from the resonantly excited state $[i]nl$ can be described as

$$A[i]nl\,* \xrightarrow{P^{q}(nl)} A^{q+} \quad \text{for} \quad q = q_{\min}-1, \ldots, q_{\max}. \tag{2}$$

Note that, for cases with a nonresonant chance of producing A^{1+}, there is a possibility of resonantly producing A^{0+}. The detection of such neutrals would be very difficult.

To seek a relationship between the two processes, we formally define $P^{(q_{\min}-1)}=P^{(q_{\max}+1)}\equiv 0$ and write

$$P^q(nl) = P^q[1-\overline{S}_q(nl)] + P^{q+1}\overline{S}_{q+1}(nl) \quad \text{for} \quad q = q_{\min}-1, \ldots, q_{\max}. \tag{3}$$

The introduction of the parameters $\overline{S}_q(nl)$ is fairly general:

Almost any probability distribution $P^q(nl)$ can be derived from the distribution P^q by a unique selection of the $\overline{S}_q(nl)$. The only restrictions are that $P^q(nl)=0$ for all $q>q_{\max}$, and that $P^q\neq 0$ for all $q_{\min}\leqslant q\leqslant q_{\max}$. Hence, Eq. (3) provides a defining relation for the parameters $\overline{S}_q(nl)$ with $q_{\min}\leqslant q\leqslant q_{\max}$. The parameters $\overline{S}_{(q_{\min}-1)}(nl)$ and $\overline{S}_{(q_{\max}+1)}(nl)$ are undefined, and can formally be set to zero.

In Part I, the form of Eq. (3) was motivated by a specific model for cascade decay of the resonantly excited states. Throughout this work we refer to this model as the "spectator cascade decay" (SCD) model.

The SCD model is based on the simplistic premise that the excited Rydberg electron acts as a spectator to the ensuing cascade decay of the ionic core. The initial state $A[i]nl*$ decays as if the spectator electron were absent, reaching a set of *core* states (A_μ^{*q+}) which are stable against further ionizing decay. At this point the spectator electron (perhaps shaken to the ml orbital [7]) either remains with the core, forming the stable ion $A^{(q-1)+}$, or is ejected during a *participator* Auger step to form A^{q+}. Schematically, SCD is envisioned as

$$A[i]nl* \xrightarrow{P^q} (A^{*q+})ml^{(q-1)+} \rightarrow \begin{cases} \xrightarrow{\overline{S}_q} A^{(q-1)+} & (ml \text{ "sticks"}) \\ \xrightarrow{1-\overline{S}_q} A^{q+}+e^- & (ml \text{ "ejected"}) \end{cases}. \tag{4}$$

The parameters $\overline{S}_q(nl)$ now take on the physical interpretation of (average) sticking probabilities. The model provides a specific formula for their calculation,

$$\overline{S}_q(nl)=\frac{1}{P^q}\sum_\mu P_\mu^q \sum_{m\geqslant m_{\min}} f_{n,m}^q s(q,\mu;ml) \quad [\text{SCD model}]. \tag{5}$$

Here, P_μ^q is the probability that $A[i]^+\rightarrow A_\mu^{*q+}$, the μth excited eigenstate of A^{q+} stable against Auger decay. Hence $\Sigma_\mu P_\mu^q = P^q$, the diagram probability indicated in Eq. (1). The $f_{n,m}^q$ are the probabilities that the nl electron shakes to the ml orbital as a consequence of $q-1$ core ionizations. Finally, $s(q,\mu;ml)$ are microscopic sticking probabilities, i.e., one minus the Auger yield of the state $(A_\mu^{*q+})ml$.

In the general case, the parameters $\overline{S}_q(nl)$ are a property of the entire cascade decay. The SCD result of Eq. (5) also exhibits this feature, mixing parameters that describe the core decay process (P_μ^q and $f_{n,m}^q$) and the final state $[s(q,\mu;ml)]$.

An important point is that the SCD development introduces the $\overline{S}_q(nl)$ as probabilities, so that $0\leqslant\overline{S}_q(nl)\leqslant 1$. However, if the SCD model is (sufficiently) inadequate to describe the physics of Eq. (3), their actual values may be positive or negative—and of any magnitude. Throughout this work we refer to the $\overline{S}_q(nl)$ as "sticking probabilities," with the understanding that they may not be actual probabilities as defined by the SCD model.

In the present experiment, the probabilities that various initial cascade states are populated depends on incident photon energy. We define the energy-dependent probabilities, or "cross sections," as σ^+ the diagram cross section for the production of the ionized state $A[i]^+$, and σ_{nl}^* the resonant cross sections for exciting the states $A[i]nl*$. From these, the total resonant $\sigma*=\Sigma_{nl}\sigma_{nl}^*$ and total $\sigma_T=\sigma^++\sigma*$ cross sections are defined. For the present experiment, in which ions are recorded in coincidence with K-shell x rays, the appropriate [5] cross sections are those associated with the K shell. The initial states of the cascade are identified by the specific x-ray line; for the $K\alpha$ line we have $i\Rightarrow 2p$, and for the $K\beta$ line $i\Rightarrow 3p$ [see Sec. IV B].

With these definitions, the yield (normalized by the incident flux) of ions A^{q+} can be written as

$$Y^q=P^q\sigma_T+C^q\sigma*. \tag{6}$$

Here

$$C^q=P^{q+1}\hat{S}_{q+1}-P^q\hat{S}_q, \tag{7}$$

with

$$\hat{S}_q=\frac{1}{\sigma*}\sum_{nl}\sigma_{nl}^*\overline{S}_q(nl). \tag{8}$$

While the average sticking probabilities $\overline{S}_q(nl)$ are energy independent, their cross-section weighted averages $\hat{S}_q$ are not. For the case of the Kr K-shell, the resonances lie close in energy, and the average is dominated by the lowest states. Furthermore, as discussed in Part I, the $\overline{S}_q(nl)$ are likely to be slow functions of n. Hence, at our present level of accuracy we treat the $\hat{S}_q$ as constants, determined mostly by properties of the $5p$ and $6p$ states.

As a function of incident-photon energy then, the yield of A^{q+} is a sum of two terms: The first, proportional to σ_T, looks like the K-shell absorption edge. The second term, proportional to $\sigma*$, peaks at energies just below the edge. Since C^q may be either positive or negative, the yields show either a resonance enhancement or depletion near the edge. In Part I we found that the low-q yields exhibited the enhancement, with a discernible peak superimposed on the K-shell edge. The high-q yields showed no such structure, since the depletion only appears as a slight shift and broadening of the edge.

Since the total yield $Y_T=\Sigma_q Y^q=\sigma_T$, one can equivalently work in terms of branching ratios

$$B^q=\frac{Y^q}{Y_T}=P^q+C^q\left(\frac{\sigma*}{\sigma_T}\right). \tag{9}$$

If the production of neutral atoms ($Y^{(0)}$) were large, the experimental branching ratios would not be in accordance with Eq. (9), since the experimental Y_T would be missing the $q=0$ contribution. However, in the present case we will argue that $q_{\min}=2$ for the $[2p]$ and $[3p]$ initial states. Of some concern are the unrecorded Kr^{1+} ions, originating from the decay of resonant states; however, we believe the error to the branching ratios due to this is negligible. In Sec. V B we

reconsider the Kr^{1+} yield from our previous experiment in light of the present development.

In Part I, the coincident ion yields Y^q were found to best reflect the physics. However, in the present case we work with the branching ratios. One reason for this is that the new experiment has an improved bandpass, and the branching ratios show more structure than in the previous experiment. Additionally, to extract the absolute (rather than relative) values of $\hat{S}_q$ from the data, one is forced at some point to model the ratio σ^*/σ_T. In Part I, this ratio was estimated as its maximum possible value (unity), providing *minimum* estimates of the $\hat{S}_q$. Finally, it also turns out that fitting branching-ratio data to the σ^*/σ_T is less sensitive to model parameters than a fit of the yields to Eq. (6).

IV. ANALYSIS AND RESULTS

A. General remarks

The use of fluorescence-ion coincidence spectroscopy is convenient for preparing atomic states with a specific inner shell hole: Exciting near or above the *K*-shell threshold, radiative resonant-Raman scattering results in the production of such states accompanied by a scattered x ray characterized by the particular atomic hole state. Ideally, this scattered (or fluorescent) photon thus identifies the atomic hole $[i]$ state left behind. Any ensuing atomic measurements made in coincidence with this photon are thus determined only by these "initial" states. In this way the spectra of ionic charge states produced in coincidence with $K\alpha$ photons arise only from decay of $[2p]$ initial states, free of any confusion due to the production of higher-lying states—such as $[3p]$.

In particular, we are interested in the decay of resonantly excited states $[i]nl$ which are created near the *K*-shell threshold, and how this decay compares with that of the nonresonant state $[i]$. Here, because of the large natural width involved, and the experimental resolution, the fluorescent photon energy cannot be used to distinguish between resonant and nonresonant initial states. Instead, by studying the evolution of the decay as a function of incident-photon energy across threshold, we extract some of the average features of the problem (as outlined in the last section).

As mentioned previously, the incident energy is most conviently measured relative to the inflection point of the *K*-shell edge. However, while convienient, this point depends on the bandpass of incident radiation and is thus different from experiment to experiment. From the theoretical point of view, the best point from which to measure relative energy is the *K*-shell ionization threshold which lies several eV above the edge (see, e.g., [8]). These two energy scales are thus different by an offset

$$E_{\mathrm{edge}} = E_{\mathrm{exc}} - \Delta, \tag{10}$$

where E_{edge} is the incident energy relative to the edge and E_{exc} (excess energy) is the energy relative to threshold. What is often forgotten in the analysis of near-edge problems is that the bandpass-dependent Δ can be difficult to determine accurately: Once Δ is determined, any ensuing error in the analysis arising from an inaccuracy in Δ is usually neglected.

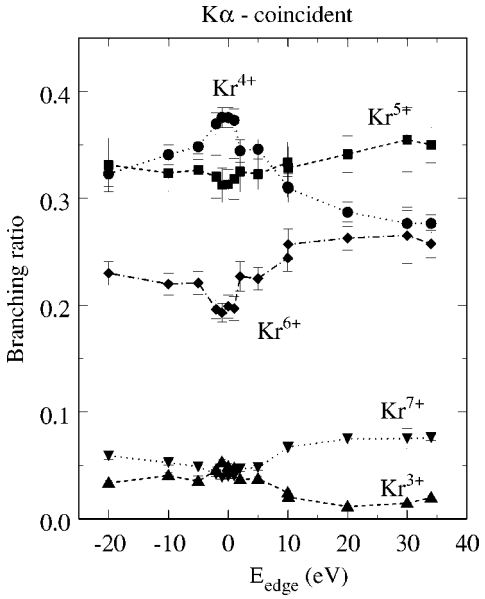

FIG. 2. Branching ratios for Kr^{q+} production in coincidence with $K\alpha$ emission, as a function of incident-photon energy. The raw data [e.g., of Fig. 1(a)] has been corrected for a charge-dependent ion detection probability. The data points are connected by lines to better indicate the trends.

Hence, in the present work we employ the experimental scale E_{edge}. Any input from theory will thus be emphasized by depending explicitly on the parameter Δ.

Coincident charge state spectra were recorded from 20 eV below the edge to 34 eV above. For each spectrum, the areas of the Kr^{q+} peaks were adjusted for the TOF efficiency and converted to branching ratios B^q. These results, for the most prominent peaks, are displayed in Fig. 2 ($K\alpha$ coincident) and Fig. 3 ($K\beta$ coincident). Because of higher statistics and lower bandpass, the branching ratios now show much more structure than those of our earlier experiment (see Fig. 2 of [5]).

B. Above-threshold results

Before analyzing the threshold behavior of the coincident charge-state distributions, it is important to establish the above-threshold branching ratios P^q. As outlined in Sec. III, these probabilities play a central role in the analysis of threshold decay. Furthermore, the ratios are important in their own right, since they provide a measure of the charge-state distributions resulting from a "pure," singly ionized state $[i]$.

To ensure that the observed branching ratios correspond to P^q, the incident-photon energy must be large enough so that $\sigma^+ \gg \sigma^*$. Hence, the energy must be larger than threshold by at least the natural *K*-shell width; $E_{\mathrm{exc}} > \Gamma_K \approx 2.7$ eV [11,12]. However, the incident energy can not be too large, since excitations of the valence shell become energetically possible. For Kr, the excitation of such states begins at $E_{\mathrm{exc}} \approx 12$ eV, where the doubly excited $[1s,4p]npn'p'$ states are produced [9]. In the present experiment, our data at $E_{\mathrm{edge}} = 10$ eV ($E_{\mathrm{exc}} \approx 5-6$ eV) fits within this energy range.

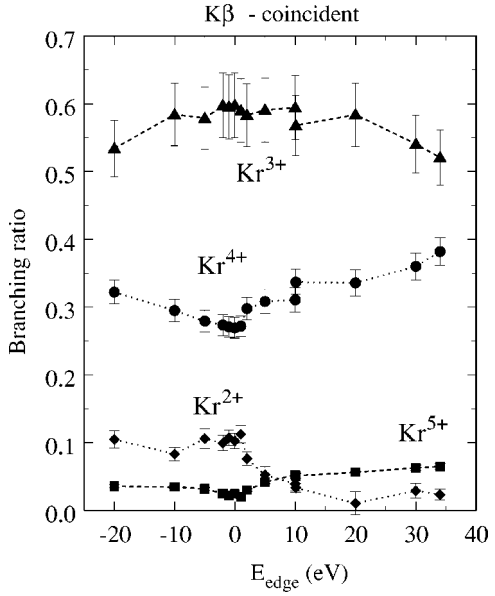

FIG. 3. Branching ratios for Kr^{q+} production in coincidence with $K\beta$ emission, as a function of incident-photon energy. The raw data [e.g., of Fig. 1(b)] has been corrected for a charge-dependent ion detection probability. The data points are connected by lines to better indicate the trends.

In the present experiment, no Kr^{1+} ions were observed because of the low $q=1$ detection efficiency. In our previous experiment, in which Kr^{q+} ions were measured in coincidence with unresolved $K\alpha$ and $K\beta$ fluorescence, Kr^{1+} was detected with a probability of $0.9\pm0.1\%$.

One pathway involving $K\alpha\beta$ emission in conjunction with Kr^{1+} production is the $K-N_{2,3}$ ($K\beta_2$) transition. The probability of $K\beta_2$ emission, relative to all $K\alpha\beta$ decay, is 1.05% [13]. When this value is adjusted to account for estimated x-ray detection efficiencies, it becomes 0.90%— in good agreement with our previous measurement. Hence, it seems likely that essentially all coincident Kr^{1+} ions produced are associated with the $[4p]$ states created in this way. This can be further verified by estimating Kr^{1+} yields using the radiative transition probabilities tabulated by Kochur *et al.* [14]: For decay beginning from $[2p]$ states $P^{(1)}\approx10^{-4}$ and from $[3p]$ states $P^{(1)}\approx2\times10^{-8}$, hence Kr^{1+} production by radiative cascade routes such as $K-L_{2,3}$ followed by $L_{2,3}-N$ is negligible.

Assuming then that all of the Kr^{1+} results from the $K\beta_2$ production of $[4p]$, *which cannot further ionize*, all $K\beta$-coincident ions with $q>1$ *must* originate from the decay of $[3l]$ states. Since the $[3d]$ contribution to the branching ratios is small $[\Gamma(K\beta_5)\approx0.0002\Gamma(K\beta_{1,3})]$ [13], we therefore associate all observed $(q>1)$ ions coincident with the $K\beta$ line as originating from the decay of $[3p]$ states. Ions coincident with $K\alpha$ decay originate from the decay of $[2p]$ states.

Table I summarizes our results. The apparent difference between our previous values and the present $[2p]$ values for $q=6$, 7, and 8 is due to the normalization requirement for each distribution. For comparison, the early work of Carlson *et al.* [16] for decay of $L_{2,3}$ vacancy states is included. These values are derived from measurements of ion yields excited

TABLE I. Above-threshold Kr^{q+} decay probabilities P^q, in percent. Column 2 displays our previously measured [5] values, which reflect a weighted average of decay from $[2p]$, $[3p]$, and $[4p]$ states. Also listed are our present results for ion abundances in coincidence with Kr $K\alpha$ (column 3) and $K\beta$ (column 5) emission. These are the branching ratios for cascade decay beginning from the $[2p]$ and $[3p]$ states, respectively. Columns 4 and 6 compare our results with the measurements of Carlson *et al.* [16] and Matsui *et al.* [10].

		$[2p]$		$[3p]$	
q	$K\alpha$, $K\beta$ average Ref. [5]	Present	Ref. [16]	Present	Ref. [10]
8	0.8 (0.3)	1.0 (0.1)	1.0		
7	5.4 (0.3)	6.7 (0.3)	8.0		
6	20.7 (0.7)	25.0 (1.0)	21.0		
5	30.1 (0.9)	33.1 (1.4)	37.0	5.2 (0.2)	5.0 (0.3)
4	32.2 (0.9)	31.0 (0.8)	29.0	32.6 (1.3)	36.3 (1.8)
3	8.6 (0.4)	2.3 (0.1)	3.0	58.6 (3.2)	56.3 (3.3)
2	1.5 (0.2)	0.8 (0.1)	1.0	3.5 (0.6)	2.3 (0.1)
1	0.9 (0.1)		<0.5		

at several energies using resonance lines, and from cross-section estimates to extract subshell yields. With their method understood, agreement with our direct results is quite good. Column 6 lists the (j-averaged) measurements of Matsui *et al.* [10] for decay of the $[3p]$ state. These values are the result of ion-yield measurements in coincidence with zero-kinetic-energy photoelectrons, as incident photon energy is swept through the M_2 and M_3 thresholds. The good agreement between their results and ours provides an independent check for our MCP efficiency corrections.

The above-threshold data are compared with theory in Fig. 4. Panel (a) displays the comparison for $[2p]$ initial vacancy states. The data of Table I is seen to be in reasonable agreement with both the (j-averaged) calculations of Kochur *et al.* [14] and those of El-Shemi *et al.* [15]. In panel (b) however, the calculations of Kochur *et al.* [14] for $[3p]$ initial states are in poor agreement with experiment; much of the theoretical Kr^{3+} intensity is shifted into observed Kr^{4+} and Kr^{5+} channels. Matsui *et al.* [10] have devoted some discussion as to the possible decay routes, which include double Auger processes.

Finally, while not included in Table I, we have observed a trace (0.4%) Kr^{6+} peak in the $K\beta$-coincident data. This charge state can not be populated from decay of $[3p]$ or $[3d]$ states due to energy conservation. Furthermore, $K-M_1$ decay is very improbable [17]—especially so here, since in two-photon decay (the main process), the two ejected photons share the transition energy which would mostly lie outside our coincidence windows. Hence, the population of $[3s]$ states can be discounted. Therefore, the Kr^{6+} $K\beta$-coincident peak most likely arises from the overlap of a weak $K\alpha$ line-shape tail and the $K\beta$ coincidence window. Any error arising from a similar effect for the $K\beta$ ions listed is negligible.

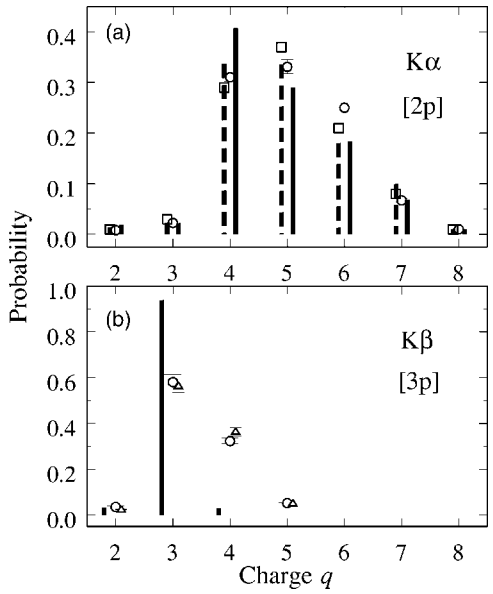

FIG. 4. Comparison of above-threshold Kr^{q+} branching ratios with theoretical predictions. Panel (a) displays our experimental results (circles) for ions coincident with $K\alpha$ emission and the experimental results of Carlson *et al.* [16] (boxes), together with the *j*-averaged $L_{2,3}$ probabilities calculated by Kochur *et al.* [14] (solid bar) and El-Shemi *et al.* [15] (dashed bar). Panel (b) displays our results (circles) for $K\beta$-coincident ions, together with the measured values of Matsui *et al.* [10] (triangles) and the calculated results of Kochur *et al.* [14] (solid bar) for decay from Kr $M_{2,3}$ states.

C. Threshold analysis

From Eq. (9), the energy dependence of the coincident Kr^{q+} branching ratios is dictated by the two parameters P^q and C^q. Once these are determined from the data, the average sticking probabilities $\hat{S}_q$ can be extracted. In keeping with our resolve to analyze the data with a minimum of theoretical modeling, we proceed differently than in Part I.

One interesting procedure along these lines involves the elimination of the unknown function σ^*/σ_T from Eq. (9), leading to linear relations between branching ratios of different charge states. A plot of B^q verses $B^{q'}$ as a function of E_{edge} produces a line whose slope is $C^q/C^{q'}$. While this procedure is completely free of any input from theory, it can only result in relative values of C^q, and thus $\hat{S}_q$. To determine them absolutely, some estimate of the cross-section ratio σ^*/σ_T is required—at least at one energy.

Determining the $\hat{S}_q$ absolutely is important; if all their values fall between 0 and +1 the validity of the SCD model is strengthened. Since modeling σ^*/σ_T can not be avoided, we proceed to model the function in the following fashion:

From total (non-coincident) ion yields scanned across the edge, we have an experimental representation of $\sigma_T(E_{\text{edge}})$. Since the ionization cross section σ^+ can be modeled with far fewer assumptions than the resonance cross section, we write $\sigma^*/\sigma_T = 1 - \sigma^+/\sigma_T$. If the transition matrix element $D_\varepsilon = \langle \text{ground}|r|[1s]\varepsilon p\rangle$ is reasonably flat for low energies (i.e., $D_\varepsilon \approx D_0$), then we may approximate [3,8]

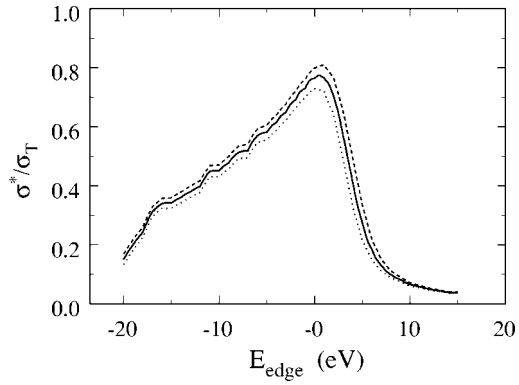

FIG. 5. Model function of Eq. (12) for the ratio of Kr *K*-shell excitation-to-total cross section. The central, solid line corresponds to an offset parameter $\Delta = 3.5$ eV. The broken lines indicate the change resulting from varying Δ by ±0.5 eV.

$$\sigma^+(E_{\text{exc}}) = \int_0^\infty \frac{|D_\varepsilon|^2 d\varepsilon}{(E_{\text{exc}} - \varepsilon)^2 + \Gamma_K^2/4} \approx \sigma^+_{\text{limit}}\left[\frac{1}{2} + \frac{1}{\pi}\tan^{-1}\left(\frac{2E_{\text{exc}}}{\Gamma_K}\right)\right], \tag{11}$$

in the near-threshold region. Here $\sigma^+_{\text{limit}} = 2\pi|D_0|^2/\Gamma_K$ is the constant, limiting value of the above-threshold cross section. (Note that this is really a scaled cross section, since throughout this work we neglect a number of constant factors for clarity.) The validity of this acrtangent approximation in the present case is inferred from the observed ion-yield above threshold: The yield has a slight positive slope (averaged) for energies $E_{\text{exc}} = 6-33$ eV. By comparing this slope with numerical simulations of σ^+ that include slowly varying models of D_ε, we estimate that σ^+ deviates from the arctangent approximation by no more than 3% of $\sigma^+(0)$ over the energy range of interest.

In terms of the incident energy relative to the edge inflection point, our model function is thus

$$\frac{\sigma^*}{\sigma_T} = 1 - \sigma^+_{\text{limit}} \frac{g(E_{\text{edge}} + \Delta)}{\sigma_T(E_{\text{edge}})}, \tag{12}$$

with

$$g(x) = \left\langle \frac{1}{2} + \frac{1}{\pi}\tan^{-1}\left(\frac{2x}{\Gamma_K}\right)\right\rangle_{\text{bandpass}}. \tag{13}$$

The brackets here denote an average over the distribution of incident-photon energies. We take the bandpass function to be Gaussian with a 2.5 eV full-width at half-maximum. The constant σ^+_{limit} is determined from the above-threshold ion yield.

Numerical experimentation shows that the function $g(x)$ is fairly insensitive to changes in the bandpass-width around 2.5 eV. The offset, Δ, between the positions of the edge and threshold, is thus the major contributor to error in the model. Figure 5 displays the resulting model for σ^*/σ_T. For the present work—with low bandpass—we use $\Delta = -3.5$ eV, in

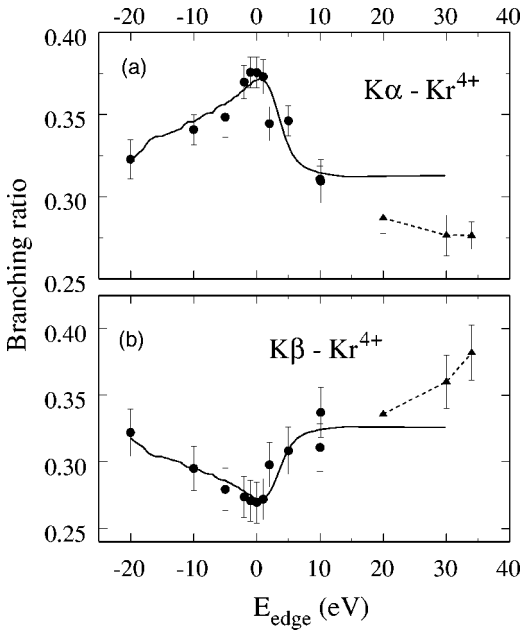

FIG. 6. Two examples of least-squares fits of branching ratios to Eq. (9) using the model function of Fig. 5. The triangular data points at high energy, connected by broken lines, are above threshold for multiple excitations and are excluded from the fit.

keeping with the work of Breinig *et al.* [8] ($\Delta \approx -3.4$). This choice corresponds to the solid curve in the figure, while the broken lines indicate how the cross-section ratio changes when Δ is varied by ±0.5 eV.

Using the model of Eq. (12), simple least-squares fits of the branching ratios to Eq. (9) provides estimates for the parameters C^q and P^q. Figure 6 displays two example fits. The high energy data, which lie above the multiple-excitation thresholds ($E_{\text{edge}} > 12$ eV), have been excluded from the fit. The fit results for $K\alpha$ and $K\beta$ coincident spectra are listed in Tables II and III, respectively.

The above-threshold branching ratios of Table I were derived assuming that the resonance cross section was negligible at $E_{\text{edge}} = 10$ eV. From Fig. 5, it can be seen that this is reasonably the case: our model indicts that $\sigma^* / \sigma_T \approx 0.05$ there. The fitted values of P^q in Tables II and III now reflect the "best" values consistent with our branching-ratio model. Within error, these probabilities still sum to unity and agree with the values of Table I.

TABLE II. Results of fitting the $k\alpha$-coincident Kr^{q+} branching ratios to Eq. (9). These parameters describe the decay of excited states associated with a $2p$ shell hole.

	[2p]	
q	C^q	P^q (%)
8	−0.0038 (0.0002)	0.93 (0.05)
7	−0.001 (0.0021)	6.29 (0.13)
6	−0.0653 (0.0128)	24.81 (0.73)
5	−0.0197 (0.0204)	33.21 (1.16)
4	0.0807 (0.0109)	30.92 (0.60)
3	0.0310 (0.0011)	2.28 (0.05)
2	0.0096 (0.0016)	0.87 (0.08)
Sum	0.0024 (0.0266)	99.30 (1.51)

TABLE III. Results of fitting the $K\beta$-coincident Kr^{q+} branching ratios to Eq. (9). These parameters describe the decay of excited states associated with a $3p$ shell hole.

	[3p]	
q	C^q	P^q (%)
5	−0.0347 (0.0026)	4.93 (0.17)
4	−0.0739 (0.0180)	32.92 (1.04)
3	0.0378 (0.0505)	56.43 (2.73)
2	0.0865 (0.0109)	3.80 (0.55)
Sum	0.0157 (0.0548)	98.08 (2.98)

With the values of Tables II and III established from the fits, the average sticking "probabilities" can be extracted recursively from Eq. (7). The recursion can proceed in either a forward or backward direction, with the accumulated error propagating in the respective directions. Our inability to detect Kr^{1+} poses a problem for beginning the forward recursion. From the discussion in Sec. IV B, there is no production of Kr^{1+} expected above-threshold (e.g., $P^{(1)} = 0$) due to decay of either the $[2p]$ or $[3p]$ states. However, near threshold there should be some Kr^{1+} yield due to spectator decay to Kr^{2+} *cores*. In particular, we have $C^{(1)} = P^{(2)} \hat{S}_{(2)}$. By definition $\Sigma C^q = 0$, hence the sum of the observed C^q ideally specifies $C^{(1)}$. In practice though, from Tables II and III it is seen the accumulated error in ΣC^q is quite large, and the sums are statistically consistent with 0. Furthermore, the sums would indicate that $C^{(1)} < 0$. While a negative $\hat{S}_{(2)}$ is allowable from the general definition, it is incompatible with our expectation that $P^{(1)} = 0$. For the moment, we assume that $C^{(1)} \ll C^{(2)}$, so the forward recursion can be started as $\hat{S}_{(3)} \approx C^{(2)} / P^{(3)}$. In Sec. V we will examine this point more carefully.

Table IV lists our results for the sticking probabilities. In Part I we devoted considerable discussion as to why it is reasonable that the $\hat{S}_q$ are increasing functions of q. This is seen to still be the case in general—but with the notable exception of decay from $[2p]np$ states to Kr^{3+}. Note also that, while the present values of $\hat{S}_q$ are still consistent with probabilities, they are larger than the "average" values we extracted in Part I. This is partly due to the approximation of Part I leading to minimum probabilities. The remainder of the increase is believed due to the large bandpass of the earlier experiment. While the bandpass was taken into account in the earlier model, the model itself was much more parameter dependent than the present one.

Finally, as mentioned above, the offset Δ causes the most notable changes in the model function (Fig. 5). However, we find the fitted values of $\hat{S}_q$ are surprisingly stable to variation in Δ. By reanalyzing the data with $\Delta \rightarrow \Delta \pm 0.5$ eV, we find the derived $\hat{S}_q$ change by no more than 0.8%.

TABLE IV. Derived values of the sticking "probabilities" $\hat{S}_q$ for decay originating from np initial states containing either a $2p$ or $3p$ hole. For each state, the recursion can go in either the forward or backward direction, with the forward recursion begun assuming $\hat{S}_2 P^2 = 0$.

	$\hat{S}_q\,[2p]$		$\hat{S}_q\,[3p]$	
q	Forward	Backward	Forward	Backward
8	0.67 (2.87)	0.41 (0.02)		
7	0.58 (0.42)	0.54 (0.04)		
6	0.41 (0.09)	0.40 (0.05)		
5	0.37 (0.04)	0.36 (0.07)	1.02 (1.11)	0.70 (0.06)
4	0.13 (0.01)	0.12 (0.09)	0.38 (0.16)	0.33 (0.06)
3	0.42 (0.07)	0.32 (1.17)	0.15 (0.02)	0.13 (0.10)
2		−0.27 (3.08)		−0.41 (1.44)

V. DISCUSSION

A. General remarks

The detailed results of the preceding section (Table IV) suggest a number of interesting points to consider. Our new value for $\hat{S}_{(3)}$ (for the $[2p]$ case) clearly violates the expected trend of increasing $\hat{S}$ with q. It also appears that, for a given $q(\neq 3)$, the sticking probability tends to decrease if the initial hole $[i]$ lies deeper in the atom. These trends have been identified previously in the decay of the two-hole Ar $[2p^2]np$ states [18].

The operational definition of $\hat{S}_q$ allows no real basis for dealing with these kinds of questions. Therefore, we must lean on the SCD model for any further insight. Although somewhat simplistic, the SCD model provides a framework for conjecture. How far any conclusions based on it can be trusted is, in itself, a matter of interest.

The SCD result for the sticking probabilities [Eq. (5)] can be rewritten as

$$\overline{S_q}(nl) = \sum_{\mu} \rho_{q,\mu} F_{q,\mu}(nl). \tag{14}$$

The ratios $\rho_{q,\mu} = (P^q_\mu / P^q)$ are the probabilities that, of all possible (diagram) cascade decay to an ion of charge q, the specific cascade $[i] \rightarrow A^{q+}_\mu$ occurs. These relative probabilities depend only on the diagram cascade process. The factors $F_{q,\mu}$ also include a weak cascade dependence (through the shake probabilities $f^q_{n,m}$), but also incorporate properties of the resonant final states $(A^{q+}_\mu)ml$ through the microscopic sticking probabilities $s(q,\mu;ml)$.

The $F_{q,\mu}$ can be estimated without excessive computation, and doing so provides further insight into the SCD model. As outlined in Part I, to proceed one makes the assumption that the microscopic sticking probabilities $s(q,\mu;ml)$ are either 1 or 0, depending on whether or not (respectively) the state $(A^{q+}_\mu)ml$ is stable against participator Auger decay. More precisely, we assume that if any participator transition $(A^{q+}_\mu)ml \rightarrow A^{q+}_\nu + e^-$ is energetically possible, then it is not only allowed but is the exclusive decay mechanism. This criteria can be determined from binding energies alone: If a state m is found stable against participator Auger decay, then all states below $(m' < m)$ are stable. Conversely, if the state m can undergo Auger decay, then all higher states $(m' < m)$ can also. Thus, there is a maximum, $m_{\max}(q,\mu)$, such that for all states $m > m_{\max}$ we have $s(q,\mu;ml) = 0$. Hence

$$F_{q,\mu}(nl) = \sum_{m_{\max} \geqslant m \geqslant m_{\min}} f^q_{n,m}. \tag{15}$$

Recall that f^q_{nm} describes the probability that the nl spectator electron shakes to the ml level as the core undergoes $q-1$ ionizing steps. Hence $F_{q,\mu}(nl)$ is the probability that the initial nl electron shakes to any state $(A^{q+}_\mu)ml$ stable against further ionization—and thus "sticks". In Eq. (15) $m_{\max}$ may be infinite (all the states are stable) and so $F_{q,\mu} = 1$ (unlike core orbitals, shake *off* of excited orbitals is quite small, see, e.g., [19]). Alternately, $m_{\max}$ may be 0 (no excited orbitals are stable) whence $F_{q,\mu} = 0$.

For example, the shake probabilities for the $q = 3$ case are estimated by

$$f^{(3)}_{n,m} = \sum_{m'=5}^{\infty} \langle np^{1+} | m' p^{2+} \rangle^2 \langle m' p^{2+} | mp^{3+} \rangle^2, \tag{16}$$

where the superscripts indicate the core charge seen by the spectator electron at a given step in the cascade. The overlaps are fairly insensitive to the particular core involved. As a test, we have calculated $f^{(3)}_{n,m}$ using configuration-average HF overlaps for two distinct core-ionization sequences: an average $2p$ decay route $[2p] \rightarrow [3d4p] \rightarrow [4p^3]$, and a fictitious valence route $[4p] \rightarrow [4p^2] \rightarrow [4p^3]$. The cumulative probabilities $F_{3,\mu}$ were found to differ between the two routes by 0.3% or less.

Hence, while the SCD parameters $F_{q,\mu}(nl)$ depend on the cascade process through their dependence on q, they are largely independent of any specific details of the cascade, e.g., the initial hole state $[i]$.

B. SCD model: Kr^{1+} yields and $\hat{S}_{(2)}$

In this subsection, we reexamine the yield of Kr^{1+} ions observed in our previous work. In the present work, we have assumed that any *above-threshold* Kr^{1+} originates from $[4p]$ decay ($K\beta_3$ coincidences). However, in the threshold region there should be a resonant production of Kr^{1+} due to $(Kr^{2+})mp$ states arising from $[2p]np$ and $[3p]np$ decay. This resonant production in turn is related to the above-threshold production of Kr^{2+}. Since Kr^{1+} ions are not measured in the present experiment, it is an important check that the new measurements of coincident Kr^{2+} be consistent with our old results for Kr^{1+}. Furthermore, to extract more accurate low-q values of $\hat{S}_q$ from our measurements, the forward recursion scheme must be used—and we must therefore have some estimate on $C^{(1)}$.

Our previous experiment did not distinguish between $K\alpha$ and $K\beta$ coincident ions. Hence, we must consider the yield

TABLE V. Parameters relevant to the SCD calculation of the sticking probabilities $\overline{S}_{(2)}(5p)$. $F_\mu(np)$ describes the probability that $[i]np \rightarrow (\mathrm{Kr}_\mu^{2+})mp$, for all m stable against ionization. The parameters ρ_μ are the relative decay probabilities to the specified cores, for $[i]=[2p]$ and $[3p]$. Finally, the sticking probabilities are calculated as $\overline{S}_{(2)}=\Sigma F_\mu \rho_\mu$.

μ	Kr_μ^{2+}	$F_\mu(5p)$	$F_\mu(6p)$	$\rho_\mu[2p]$	$\rho_\mu[3p]$
1	$[4p^2]({}^3P)$	1	1	0.362	0.293
2	$[4p^2]({}^1D)$	0.997	0.987	0.301	0.275
3	$[4p^2]({}^1S)$	0.743	0.086	0.085	0.093
$\geqslant 4$	$[4s4p]$ and $[4s^2]$	0	0	0.252	0.339
	$\overline{S}_{(2)}(5p)$			0.725	0.637
	$\overline{S}_{(2)}(6p)$			0.666	0.572

of Kr^{1+} from $[2p]$, $[3p]$, and $[4p]$ hole states. (Contributions from the $[3d]$ state are found negligible.)

Consider first the Kr^{1+} yield associated with the $[4p]$ state. Since this state is stable, there is a nonresonant (diagram) yield $Y^{(1)}=1\times\sigma^+$. There is no resonant contribution ($\propto\sigma^*$) since there is no possibility of the resonant $[4p]mp$ states ionizing ($\hat{S}_{(1)}=1$). (These states thus produce a neutral yield $Y^{(0)}=1\times\sigma^*$.)

Of the remaining initial hole states, nonresonant production of Kr^{1+} is quite small [Sec. IV B]. Hence, any production of Kr^{1+} originating from these hole states is almost entirely due to the resonant route $[i]np\rightarrow[4l,4l']mp$.

The theory outlined above can easily be applied to the case of $(Kr^{2+})mp$. In fact, the SCD model should be most applicable in this situation. The basic tenet of the model, in the present context, is that the probability of $[i]np\rightarrow[4l]$ participator Auger decay is very unlikely in comparison with $[i]np\rightarrow[4l,4l']mp$ spectator decay. The resonant production of Kr^{1+} thus depends on the probability that the mp electron sticks to the Kr^{2+} core.

To test this basic SCD hypothesis, we have calculated partial rates for the spectator and participator channels. These calculations were preformed in LS-coupling using relaxed, configuration-average HF wavefunctions, with a statistical average over initial substates. For the $[2p]5p$ initial states, the total spectator and participator partial rates are 6.7×10^{-2} and 4.1×10^{-4} ma.u., respectively. Similarly, the $[3p]5p$ transition rates are 2.6 and 1.7×10^{-2} ma.u. In either case, the ratio of participator to spectator probability is $\approx$0.006, and so the basic SCD premise is apparently justified. However, it should be noted that participator transitions are not necessarily weak compared to every spectator transition: for example, the $[3p]5p$-$[4p]$ rate is comparable to that of the weak $[3p]5p$-$[4s^2]5p$ transition (1.5×10^{-2} mau).

With the SCD model justified, the Kr^{1+} yield from the $[2p]$ and $[3p]$ hole states is then $Y^{(1)}=P^{(1)}\sigma_T+C^{(1)}\sigma^*\approx P^{(2)}\hat{S}_{(2)}\sigma^*$. Table V lists the ingredients needed to calculate the $q=2$ sticking probability for the $5p$ and $6p$ resonant states. The relative probabilities ρ_μ are derived from our HF rate calculations mentioned above. The parameters F_μ have been calculated as outlined in the last subsection. The difference in $F_{(3)}$ between the $5p$ and $6p$ cases is due to the fact that the $6p$ orbital shakes to higher levels than the $5p$. Thus, on average the final mp orbital is less tightly bound in the $6p$ case, and can thus take better advantage of the $({}^1S)$-$({}^3P)$ multiplet splitting to ionize. Since the resonant cross section is dominated by the $5p$ state, we approximate $\hat{S}_{(2)}\approx\overline{S}_{(2)}(5p)$.

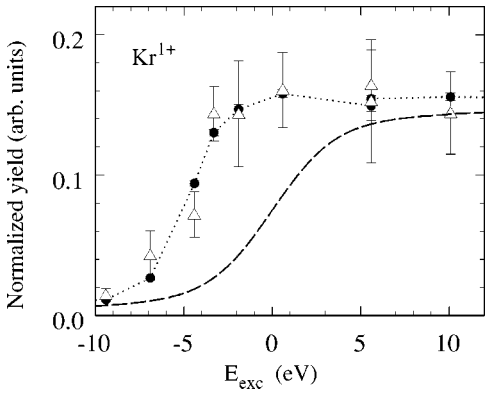

FIG. 7. Flux normalized yield of Kr^{1+} ions (triangles) coincident with $K\alpha$, $K\beta$ fluorescence, as a function of incident photon energy across the K-shell edge. The circles connected by dotted lines are the total-ion edge σ_T, scaled to the Kr^{1+} yield. The dashed line is an estimate of σ^+, the ionization component of the edge. If there were no contribution from resonant $[2p]np$ and $[3p]np$ initial states, the yield would follow σ^+.

The $[2p]$ and $[3p]$ yields can then be computed using our measured values of $P^{(2)}$. Each of the $[2p]$, $[3p]$, and $[4p]$ yields are weighted by the relative branching ratios of $K\alpha$, $K\beta_{1,3}$, and $K\beta_2$ decay [13], respectively, corrected for detector efficiency. Finally, we arrive at the expected Kr^{1+} yield for our previous experiment:

$$Y^{(1)} = 0.0106\sigma^+ + 0.0095\sigma^*. \tag{17}$$

The first term arises almost entirely from the decay to $[4p]$ diagram states. The second term is due chiefly to decay of $[2p]np$ and $[3p]np$ resonant states. If $[i]np$ participator decay is included, an additional term $0.0003\sigma^*$ is added. Hence, a fortuitous combination of resonant and diagram contributions from different initial hole states results in a Kr^{1+} yield proportional to the total cross section: $Y^{(1)}\approx0.01\sigma_T$. Figure 7 displays our previous results for $Y^{(1)}$, together with the scaled total-ion edge, proportional to σ_T. The agreement between both sets of data confirms our expectations of Eq. (17). Also shown in the figure is an estimate of σ^+, derived from the convolution of Eq. (13) with the experimental bandpass.

The application of the SCD model to the tractable case of Kr^{1+} thus provides a fairly detailed and consistent interpretation of our earlier results. Hence, we are reasonably confident in using the SCD results for $\hat{S}_{(2)}$ to reexamine the forward recursion scheme, which derives values of $\hat{S}_q$ from our measured C^q.

TABLE VI. Best values for the sticking probabilities. These are our results from either the backward or corrected-forward recursion values. The values for $q=2$ are calculated from the SCD model.

	"Best" $\hat{S}_q$	
q	$[2p]$	$[3p]$
8	0.41(2)	
7	0.54(4)	
6	0.40(5)	
5	0.39(3)	0.70(6)
4	0.15(1)	0.33(6)
3	0.71(8)	0.19(2)
2	0.73	0.64

From the preceding discussion we have SCD estimates for $C^{(1)}=P^{(2)}\hat{S}_{(2)}$: $C^{(1)}=0.0066\pm0.0009$ for the $[2p]$ case, and $C^{(1)}=0.0223\pm0.0038$ in the $[3p]$ case. Here, the uncertainty comes from our measured values of $P^{(2)}$. Contrary to our earlier assumption, these are not negligible in comparison with our measured values of $C^{(2)}$ (Tables II and III). Beginning the forward recursion using these new values has little effect on most of the corrected values of $\hat{S}_q$, except for increasing $\hat{S}_{(3)}$ dramatically in the $[2p]$ case. In Table VI we collect the "best" values for $\hat{S}_q$. These are values with minimum error, taken from either the backward or the forward recursion scheme, started with the SCD estimate of $\hat{S}_{(2)}$.

The results of Table VI show that our "general" trend of Part I (*viz.* increasing sticking probability with increasing q) is now clearly violated for both the of $[2p]$ and $[3p]$ decay. Instead, we find that $\hat{S}_q$ is large for the lowest values of q, drops dramatically, and then increases—perhaps becoming constant for the larger values of q.

C. SCD model: $\hat{S}_{(3)}$

If the SCD model is applicable for the $q=2$ case, what about the case of $q=3$? This situation is particularly interesting since the value of $\hat{S}_{(3)}$ decreases as $[i]$ becomes less tightly bound, contrary to all other cases.

Before proceeding, a few remarks on how applicable the SCD model is to the $q=3$ case are in order. Specifically, are participator channels negligible in the first and second steps of the ionization? The resonant decay paths to the states $(\mathrm{Kr}_\mu^{3+})mp$, which predominantly determine $\hat{S}_{(3)}$, follow the route $[i]np\rightarrow[f,4l]m'p\rightarrow[4l^3]mp$. We have seen that participator decay in the first decay step is reasonably small in comparison with the spectator transitions of interest here. The question thus centers on the relative probability of participator decay from the resonant intermediate states. However, such transitions are of the from $[f,4l]m'p\rightarrow[4l]+e^-$, and would lead to the resonant production of Kr^{1+}. Since the probability of $[i]\rightarrow[f,4l]$ is much larger than that of $[i]\rightarrow[4l^2]$ considered in the last section, any significant participator decay from $[f,4l]m'p$ resonant states would produce a large contribution to resonant Kr^{1+} yield (which is already adequately described), we conclude that participator transitions are again negligible.

To proceed with the SCD calculation of decay to Kr^{3+}, we first identify the *core* states Kr_μ^{3+} that are stable against Auger decay. Within the single-configuration HF scheme, these are the eight LS-coupled valence states with three holes: $[4p^3]$, $[4s4p^2]$, and $[4s^24p]$. Of these states, it must be determined for which values of m the resonant states $(\mathrm{Kr}_\mu^{3+})mp$ are energetically stable against participator Auger decay.

The calculation for $F_{3,\mu}(nl)$ proceeds in a similar manner to the $q=2$ case. Because the $[4p^3]$ multiplet splitting is comparable to that of the $[2p^2]$ configuration, while the np binding energy is increased due to the larger core charge, $F(5p)\approx1$ for all three $[4p^3]$ substates. However, the binding energy is small enough that $F(5p)=0$ for any of the $[4s4p^2]$ or $[4s^24p]$ inner-valence states. Thus, the $5p$ initial orbital is "stuck" if the core cascade ends in any of the $[4p^3]$ states. Again, taking $\hat{S}_{(3)}\approx\overline{S}_{(3)}(5p)$, we have the simple result that $\hat{S}_{(3)}$ is the probability of diagram cascade $[i]\rightarrow[4p^3]$, relative to all $[i]\rightarrow[4l,4l',4l'']$ transitions.

Unlike the $q=2$ case, the probabilities $\rho_{(3),\mu}$ cannot be easily calculated. However, we are only concerned with the probability of all $[N_{2,3}N_{2,3}]$ states, which can be estimated using the closed-shell decay probabilities of Kochur *et al.* [14]. The decay probabilities can be traced for each cascade step, roughly correcting the probabilities in the second step to account for open subshells [21]:

The first step of $[3p]$ cascade decay, resulting in Kr^{3+}, must be $[3p]\rightarrow[3d,4l]$. The Kr^{3+} is a major decay product of $[3p]$ decay because of this strong Coster-Kronig channel. The $3d$ hole then decays via $[3d]\rightarrow[4l',4l'']$ forming $[4l,4l',4l'']$. We estimate that the $[4p^3]$ states are populated with a probability of 0.13 relative to all diagram cascade $[3p]\rightarrow\mathrm{Kr}^{3+}$. While this value roughly agrees with our measured $\hat{S}_{(3)}\approx0.19$, the agreement may be fortuitous since the scheme also predicts an absolute Kr^{3+} probability $P^{(3)}=97\%$—in very poor agreement with the measured value of 59%. The work of Matsui *et al.* [10] implies that much of this "excess" Kr^{3+} probability is dispersed to higher charge states due to a $[3p]\rightarrow[3d,4p^2]$ double Auger decay in the first step. If this is the case, then our *relative* probabilities $\rho_{(3),\mu}$ would remain unchanged and the SCD model would apply. Note that in this case, the SCD model would require a slight modification for $q>3$ to account for high-probability double ionization steps.

Decay from the $[2p]$ state forming Kr^{3+} is much more complicated than from the $[3p]$ state. However, the cascade is still largely dominated by $[2p]\rightarrow[3d,4l]$ in the first step. In this case we estimate the relative probability of the $[4p^3]$ states is 0.18, in very poor agreement with our measured value of $\hat{S}_{(3)}\approx0.71$. Here, the estimated absolute probability $P^{(3)}=2.2\%$ agrees well with our measured value.

While the estimate for the $[2p]$ value of $\hat{S}_{(3)}$ is in poor agreement with our measurement, the trend is correct: $\hat{S}_{(3)}$ is

TABLE VII. Average charge, sticking probability, and their ratio for Kr $[2p]np$ and $[3p]np$ decay.

	$[2p]$	$[3p]$
$\langle q\rangle_d$	4.99 (0.08)	3.33 (0.09)
$\langle\hat{S}_q\rangle_d$	0.34 (0.17)	0.27 (0.16)
$\langle\hat{S}_d\rangle_d/\langle q\rangle_d$	0.068 (0.034)	0.081 (0.048)

larger in $[2p]$ case than in the $[3p]$ case. This feature stems from the fact that $[4p^3]$ valence configurations are populated more often in $[2p]\rightarrow Kr^{3+}$ than in $[3p]\rightarrow Kr^{3+}$ cascade decay.

D. Average charge

What can be said about the present results in light of the *general* (or operational) definition of $\hat{S}_q$ [i.e., Eqs. (3) and (8)]? The state-specific, average sticking probabilities are given by

$$\overline{S}_{q+1}(nl)=\frac{1}{P^{q+1}}\sum_{q'=q_{\min}}^{q}[P^{q'}(nl)-P^{q'}]. \tag{18}$$

If $\overline{S}_{q+1}(nl)>0$, the cumulative probability for $[i]nl\rightarrow A^{q+},A^{(q-1)+}\ldots, A^{q\min+}$ must be greater than that for $[i]\rightarrow A^{q+},\ldots, A^{q\min}$. In terms of a causal relationship $P^q\Rightarrow P^q(nl)$, a positive "sticking probability" implies a transfer of nonresonant probability to lower charge states. This is the generalized notion of the spectator electron sticking.

The only physical interpretation of the $\overline{S}_q(nl)$, outside of the SCD model, is that their average indicates a shift in average charge between diagram and resonant cascade:

$$\langle q\rangle_{nl}=\langle q\rangle_d-\langle\overline{S}_q(nl)\rangle_d. \tag{19}$$

Here, the subscripts *nl* and *d* refer to averages with respect to the resonant $P^q(nl)$ and diagram P^q probability distributions, respectively. Thus, a positive *average* $\overline{S}_q$ indicates a decrease in the resonant average charge. The average of $\hat{S}_q$ thus implies the decrease in average charge for the cross-section-averaged collection of all *nl* resonant states.

Table VII displays the average charge and sticking probability associated with the $[2p]$ and $[3p]$ initial states, derived from the results of the last section. Also shown is their ratio, which is similar for either initial state hole (within the large uncertainty). While this result may be coincidental, it suggests the empirical relation $\langle q\rangle_{nl}\approx 0.93\langle q\rangle_d$, regardless of *nl* or the type of initial hole.

E. Further speculation

The preceding analysis and discussion makes clear that, while the parameters $\overline{S}_q(nl)$ are well defined, in practice they are difficult to extract from experiment. In simple cases, where there are isolated resonances below threshold, the job is much easier. This is the case for the Ar *K*-shell edge: where the $4p$ resonance is conspicuous it is possible to isolate $\overline{S}_q(4p)$ and $\overline{S}_q(5p)$ associated with the double-hole initial states Ar $[2p^2]np$ [18]. However, for cases such as the present Kr example, a number of approximations must be made, and a variety of subtleties arise. How can the present results and conclusions be confirmed or tested?

The case of Kr^{1+} yields is clearly an important one, because an accurate knowledge of $\hat{S}_{(2)}$ is necessary to extract values of $\hat{S}_q$ for higher q. Hence, future work should be careful to acquire Kr^{1+} data with sufficient statistics, preferably distinguishing between $[3p]$ and $[4p]$ initial holes (i.e., $K\beta_{1,3}$ and $K\beta_2$ coincidences). The SCD predictions outlined above are consistent with our previous data, which is a composite of $[2p]$, $[3p]$, and $[4p]$ decay. It would be an important step to verify these predictions for the individual cases: $[2p]$ and $[3p]$ yields should only have resonant components, and the $[4p]$ yield only a diagram component.

The comparison of $\hat{S}_q$ between different initial holes $[i]$ is also interesting. If the $\hat{S}_q$ are to prove useful parameters in describing generalities of cascade decay, this is an important consideration. For fixed q, the final states and number of ionization steps is independent of the initial hole. Hence the change in $\hat{S}_q$ with $[i]$ must be strongly related to how the population of these final states differs between the different cascades. For the $q=3$ case, we have seen that the SCD model goes further to directly link the parameter $\hat{S}_{(3)}$ as the probability of diagram $[i]\rightarrow[4p^3]$, relative to all $[i]\rightarrow[4l^3]$ decay. This could, in principle, be confirmed by measuring the UV decay of $[4s^2,4p]$ and $[4s,4p^2]$ to $[4p^3]$ in coincidence with Kr^{3+}. A number of very real practical difficulties would have to be dealt with, however.

VI. CONCLUSION

We have reported new measurements of Kr^{q+} ions, now coincident with either $K\alpha$ or $K\beta$ fluorescence. Because of the improved bandpass of the present experiment, much more detail is apparent in the behavior of the ion branching ratios as incident-photon energy is swept through the Kr *K*-shell threshold.

From the branching ratios just above threshold, we have obtained new measurements of the ion charge-state probabilities for decay from the Kr $[2p]$ and Kr $[3p]$ states. The $[3p]$ probabilities are in good agreement with those measured by Matsui *et al.* [10]. Our measured probabilities for the $[2p]$ state are found to be in reasonable agreement with the calculated values of both Kochur *et al.* [14] and El Shemi *et al.* [15].

The behavior of the branching ratios in the threshold region have been outlined theoretically. A new method of threshold analysis, requiring as little as possible support from theory, has been presented and applied to the data. This analysis extracts the average sticking probabilities $\hat{S}_q$, which we feel are a useful set of parameters for investigating the general relationship between cascade decay from resonant and nonresonant hole states. We report the results for $q=2-8$ for the $[2p]$ case and for $q=2-5$ for the $[3p]$ case.

Using a simplified model, we have computed $\hat{S}_q$ for $q=2$ for the relevant cases, and reanalyzed our old data in light of these results. Our calculated values of $\hat{S}_{(2)}$ were found to adequately describe our old Kr^{1+} results. These theoretical results were employed to correct some of the fitted estimates, and we have presented a table of our "best" estimates for the sticking probabilities. We find the sticking probabilities violate the "general" trend (of increasing $\hat{S}_q$ with increasing q) proposed in our earlier work. Computation for the $q=2$ and $q=3$ cases reveals that this violation is consistent with our simplified model of decay. Finally, we have presented some speculation on future work needed.

ACKNOWLEDGMENTS

This work was supported by the National Science Foundation at the University of Tennessee. We are grateful to the staff of the Basic Energy Sciences Synchrotron Radiation Center at the Advanced Photon Source for their assistance in performing the experiments. The Argonne group was supported by the Chemical Sciences, Geosciences, and Biosciences Division of the Office of Basic Energy Sciences, Office of Science, U. S. Department of Energy, under Contract No. W-31-109-ENG-38. Use of the Advanced Photon Source was supported by the U. S. Department of Energy, Basic Energy Sciences, Office of Science, under Contract No. W-31-109-ENG-38.

[1] T. Åberg and J. Tulkki, in *Atomic Inner-Shell Physics*, edited by B. Crasemann (Plenum, New York, 1985), p. 419.
[2] B. Crasemann, Comments At. Mol. Phys. **22**, 163 (1989).
[3] G. B. Armen, in *X-Ray and Inner-Shell Processes*, edited by A. Bianconi, A. Marcelli, and N. L. Sani (AIP, Melville, NY, 2003), p. 3.
[4] M. A. MacDonald, S. H. Southworth, J. C. Levin, A. Henins, R. D. Deslattes, T. LeBrun, Y. Azuma, P. L. Cowan, and B. A. Karlin, Phys. Rev. A **51**, 3598 (1995).
[5] G. B. Armen, E. P. Kanter, B. Krässig, J. C. Levin, S. H. Southworth, and L. Young, Phys. Rev. A **67**, 042718 (2003).
[6] M. A. Beno, C. Kurtz, A. Munkholm, U. Rütt, M. Engbretson, G. Jennings, J. Linton, G. S. Knapp, and P. A. Montano, Nucl. Instrum. Methods Phys. Res. A **467-468**, 694 (2001).
[7] We treat the spectator excitation here—mostly for notational convenience—in the simplest possible way as a sudden transition in which the angular momentum of the orbital l does not change.
[8] M. Breinig, M. H. Chen, G. E. Ice, F. Parente, B. Crasemann, and G. S. Brown, Phys. Rev. A **22**, 520 (1980).
[9] S. J. Schaphorst, A. F. Kodre, J. Ruscheinski, B. Crasemann, T. Åberg, J. Tulkki, M. H. Chen, Y. Azuma, and G. S. Brown, Phys. Rev. A **47**, 1953 (1993).
[10] T. Matsui, H. Yoshii, A. Higurashi, E. Murakami, T. Aoto, T. Onuma, Y. Morioka, A. Yagishita, and T. Hayaishi, J. Phys. B **35**, 3069 (2002).
[11] M. O. Krause and J. H. Oliver, J. Phys. Chem. Ref. Data **8**, 329 (1979).
[12] M. H. Chen, B. Crasemann, and H. Mark, Phys. Rev. A **21**, 436 (1980).
[13] LBNL Isotopes Project—LUNDS Universitet Nuclear Data Dissemination Home Page, Lawrence Berkeley National Laboratory, http://ie.lbl.gov/toi.htm. See also http://nucleardata.nuclear.lu.se/NuclearData/toi, which lists slightly different Kr decay probabilities, whence the $K\beta_2$ probability relative to all $K\alpha\beta$ decay is 0.95%.
[14] A. G. Kochur, V. L. Sukhorukov, A. I. Dudenko, and Ph V. Demekhin, J. Phys. B **28**, 387 (1995).
[15] A. El-Shemi, Y. Lofty, and G. Zschornack, J. Phys. B **30**, 237 (1997).
[16] T. A. Carlson, W. E. Hunt, and M. O. Krause, Phys. Rev. **151**, 41 (1966).
[17] R. W. Dunford, E. P. Kanter, B. Krässig, S. H. Southworth, and L. Young, Phys. Rev. A **67**, 054501 (2003).
[18] J. C. Levin and G. B. Armen, Radiat. Phys. Chem. **70**, 105 (2004).
[19] G. B. Armen, J. Phys. B **29**, 677 (1996).
[20] G. B. Armen and F. P. Larkins, J. Phys. B **24**, 741 (1991).
[21] T. Åberg and G. Howat, in *Corpuscles and Radiation in Matter I*, edited by S. Flügge and W. Mehlhorn, Handbuch der Physik Vol. XXXI (Springer, Berlin, 1982), p. 469. (See Eqs. 9.21-9.22. Note that these are actually corrections to partial rates. To correct branching ratios, the corrections must be made to all possible transitions, followed by renormalization of the total probability to unity.)